Fractal-based autonomous partial discharge pattern recognition method for MV motors

Ma, Zhuo; Yang, Yang; Kearns, Martin; Cowan, Kevin; Yi, Huajie; Hepburn, Donald M.; Zhou, Chengke

Published in:
IET High Voltage

DOI:
10.1049/hve.2017.0109

Publication date:
2018

Document Version
Peer reviewed version

High Voltage

Research Article

IET Journals
The Institution of Engineering and Technology

Fractal-based autonomous partial discharge pattern recognition method for MV motors

ISSN 2397-7264
Received on 20th July 2017
Revised 13th October 2017
Accepted on 22nd November 2017
E-First on 25th January 2018
doi: 10.1049/hve.2017.0109
www.ietdl.org

Zhuo Ma[1], Yang Yang[1], Martin Kearns[2], Kevin Cowan[2], Huajie Yi[1], Donald M. Hepburn[1], Chengke Zhou[1] ✉

[1]*School of Engineering and Built Environment, Glasgow Caledonian University, Glasgow, G4 0BA, UK*
[2]*Electrical System Group, Engineering Division, Nuclear Generation, EDF Energy, Glasgow, G74 5PG, UK*
✉ *E-mail: c.zhou@gcu.ac.uk*

Abstract: On-line partial discharge (PD) monitoring is being increasingly adopted to improve the asset management and maintenance of medium-voltage (MV) motors. This study presents a novel method for autonomous analysis and classification of motor PD patterns in situations where a phase-reference voltage waveform is not available. The main contributions include a polar PD (PPD) pattern and a fractal theory-based autonomous PD recognition method. PPD pattern that is applied to convert the traditional phase-resolved PD pattern into a circular form addresses the lack of phase information in on-line PD monitoring system. The fractal theory is then presented in detail to address the task of discrimination of 6 kinds of single source and 15 kinds of multi-source PD patterns related to motors, as outlined in IEC 60034. The classification of known and unknown defects is calculated by a method known as centre score. Validation of the proposed method is demonstrated using data from laboratory experiments on three typical PD geometries. This study also discusses the application of the proposed techniques with 24 sets of on-site PD measurement data from 4 motors in 2 nuclear power stations. The results show that the proposed method performs effectively in recognising not only the single-source PD but also multi-source PDs.

1 Introduction

Partial discharge (PD) activity within a rotating machine is not only an indication of an insulation defect but also a causative mechanism of further insulation deterioration. Standard patterns of PD activity have been developed to allow identification of a fault. Automatic PD detection and source classification is becoming increasingly important in on-line insulation condition assessment of motors [1, 2]. Monitoring a motor in service and diagnosing the insulation condition by using recognition approaches from acquired PD is desirable [3, 4]. However, different sources of PD could be detected under on-line measurement. Different sources of PD are of different risks and complex conditions, such as slot type PD would be high risk with low-to-medium PD magnitude, but surface type PD would be a medium risk with high PD magnitude. There is high demand in the industry to distinguish multiple PD sources. However, there are several challenges to achieve the recognition of motor PD patterns automatically.

It has been identified that different PD types generate different PD patterns [5]. The PD pattern is represented by a set of characteristic attributes, which are extracted from measured PD raw data. According to different attributes, PD pattern is commonly classified into two types for analysis and classification: phase-resolved data and time-domain data [6]. Currently, the most widely used method is based on the analysis of phase-resolved PD (PRPD) data, which has three parameters φ, q, n. Here φ is the voltage phase angle at which the PD occur (normally assigned as 5° or 10° windows), q is the measured PD magnitude and n is the number of PDs which occur in the phase window over a defined number of measurements. PRPD patterns are considered to be a reliable indication of the root cause of an insulation fault. Recognition of multiple PD sources was introduced in [7, 8], it was found that high recognition rate only occurs with multi-source PDs with highly different PRPD patterns, in terms of shapes and polarities, whereas, multiple PDs with similar PRPD patterns were found to be more difficult to distinguish [9–12]. However, the reference voltage waveform is hard to obtain in on-line monitoring condition. The loss of φ makes it impossible to use PRPD pattern in PD recognition in motors.

Pattern recognition technology has been studied and applied in PD pattern recognition in the last few decades [13, 14]. Various artificial intelligence (AI) techniques such as artificial neural network, knowledge-based system, and support vector machines have been applied to PRPD pattern classification [15, 16]. AI approaches require a large number of data for training and learning, and training data should be 'healthy' to ensure a good result. Other techniques, such as distance classification technique and fuzzy logic, are also used for PD source classification [17, 18]. Most of the techniques introduced above provide promising fault recognition results when only one PD type exists but perform less well when multiple sources are considered. Moreover, most of these approaches, which required a massive amount of data for training and testing, were tested and validated on one specific motor under laboratory conditions. Their general application to practical on-line situations has not yet been investigated.

In a practical on-line situation, the three challenges in this paper when attempting autonomous PD pattern classification in motor condition assessment could be summarised as follows: (i) processing PD pattern without voltage phase information [19]; (ii) establishing a general pattern classification reference suitable for practical applications; (iii) recognising multiple PD sources, which may occur in a medium-voltage (MV) motor simultaneously.

This paper investigates autonomous pattern recognition techniques for motor PD classification. To address the key challenges mentioned above, a novel pattern recognition framework is presented in the paper. Polar PD (PPD) representation, which converts a PRPD to a circular format, is applied to address the loss of voltage phase information. Moreover, the phase shift often causes a cluster of PD pulses, of which the integrity is essential for many established PRPD pattern recognition techniques, into two halves, one at the beginning of the PRPD pattern, and the other at the end [19]. For this reason, the PRPD patterns will be converted to PPD pattern which connects the beginning of a 50 Hz, alternating current (AC) cycle of PD data with the end of the dataset. PPD pattern images form the standard defects reference converted from PRPD images of the six PD types from IEC 60034-27 [20]. Fractal theory is applied to extract proper

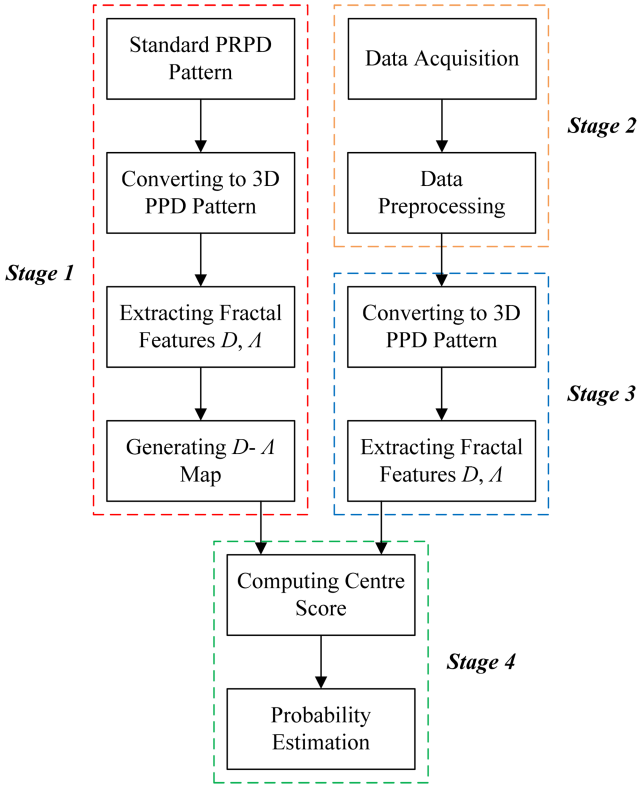

Fig. 1 *Schematic of proposed fractal-based PD pattern recognition method*

fractal features of both single-source and multi-source PD types. Centre score (CS) algorithm [3], a conventional PD source classification method which performs high recognition rate without data training, is implemented for PD source classification. Extensive laboratory experiments and on-site tests are conducted using artificial PD geometries to verify the feasibility of the developed system.

In the next section of this paper, it reviews the fractal theory-based PPD pattern recognition framework for PD source classification. In Section 3, PRPD-to-PPD conversion is introduced. Then the box-counting method (BCM)-based fractal analysis is introduced to extract the fractal features from three-dimensional (3D) PPD pattern images in Section 4. Section 5 presents the fractal map based on IEC standard PRPD patterns. The CS algorithm for PD source classification is introduced for evaluating the possibility of PD sources in Section 6. Section 7 describes the experimental setup for validating the proposed method. Finally, Section 8 presents the application of the proposed method to practical on-site test data before the conclusions are provided in Section 9.

2 Pattern recognition framework for PD source classification

This paper focuses on the establishment of a pattern recognition method which can recognise the standard motor PD patterns as given in IEC 60034. As shown in Fig. 1, the proposed PD pattern recognition consists of four main stages.

Stage 1 is the establishment of PD pattern recognition reference. At this stage, firstly, six standard types of motor PDs from IEC 60034-27 are converted from 3D PRPD patterns to 3D PPD patterns. Then, a fractal map (lacunarity versus fractal dimension) based on the 3D PPD patterns is generated using the BCM-based fractal theory.

In Stage 2, raw data is detected either in laboratory or field through high-frequency current transformers (HFCTs) and high-pass filters. These raw data are then pre-processed before the extraction of fractal features. In the pre-processing procedure, de-noising is carried out before a 3D PRPD image is generated for a PD dataset. The de-noising technique applied in the present work can be referred to in [21, 22].

In Stage 3, the pre-processed PD data in 3D PRPD patterns is converted to 3D PPD patterns, which consists of PD pulse magnitude and pulse number distribution with respect to time within the sampling period. Then two fractal features (fractal dimension D and lacunarity Λ) are determined from the 3D PPD pattern using the BCM-based fractal theory.

In Stage 4, CSs of the set of fractal features (D, Λ) from Stage 3 are calculated based on the fractal map to recognise motor PD sources to estimate the probability of motor PD sources.

3 PRPD-to-PPD pattern conversion

Before extracting the fractal features of a PD pattern, the pre-processed PD data is firstly converted to a 3D PRPD pattern. In IEC 60034, the given PRPD pattern is 3D where phase information $\varphi$is in abscissa and PD amplitude is in ordinate. The information of n, the number of PDs, is indicated by different colours.

To avoid the influence of the loss of reference voltage phase, 3D PPD pattern is considered in the on-site test data. In the previous study as introduced in [19], it is hard to acquire a reference voltage signal in on-line monitoring. The only applicable voltage is the low-voltage (LV) power supply as a reference, with data acquisition being triggered at the 0° (positive zero-crossing) point of the LV power supply. The present authors have carried out PD measurements in six power stations. The experience is that the phase shift between the motor working voltage and the LV power supply varies in different power stations. Although this LV zero-crossing provides a synchronised reference for data capture, an unknown phase shift exists relative to the waveform of the motor working voltage.

The relative phase information is kept in a circular format. The number of PDs occurring in each pixel position is added over the number of records taken during a test and a φ–q–n pattern becomes an x–y–n pattern.

The conversion from 3D PRPD patterns to 3D PPD patterns is as follows. The data point in a 3D PPD pattern image is calculated from

$$\begin{cases} x = fix(r \cdot \cos\theta) + c \\ y = fix(r \cdot \sin\theta) + c \\ z = n \end{cases} \quad (1)$$

where θ represents the phase information of a PD pulse, which is extracted from the time instant of each pulse in the 20 ms data record gathered; r represents the normalised PD pulse in the polar coordinate system; n represents the count or number of PDs which occurs in the phase window over a defined number of measurements; x, y represent the pixelated positions of each PD; c is a constant value which makes all the values of x and y equal or greater than zero. In a PPD image of a resolution of 128×128, c equals to 128 for the convenience of observation that the polar origin is in the centre of the image; the z-axis represents the PD count n.

4 BCM-based fractal analysis

4.1 Brief overview of fractal theory

Fractal theory is an image processing technique. Mandelbrot in [23] first developed the concept of fractal geometry which was applied to the model and describe natural shapes and phenomena with a brand new dimension known as 'self-similarity' [24, 25]. Fractal dimension (FD) measures the geometrical complexity of images. However, it has been observed that FD alone is insufficient for purposes of discrimination since the two surfaces of different appearance could have the same value of FD. So, Lacunarity, Λ, was introduced as a measure of spatial heterogeneity. Beyond being an intuitive measure of gaps, lacunarity can quantify additional features of patterns such as 'rotational invariance' and more generally, heterogeneity [26, 27].

PD activity is also considered as a natural phenomenon occurring in electrical insulation system due to inhomogeneity in the insulation material and gives rise to a variety of complex shapes in its PRPD patterns [28]. According to IEC 60034-27, motor PD sources have different PRPD pattern shapes and this provides a way to distinguish PD sources by comparing their PRPD pattern shapes. The complexity of the shape of a 3D PRPD or a 3D PPD pattern image can be represented by fractal geometry [29]. It shows the possibility to apply the proposed fractal analysis with fractal dimension and lacunarity to recognise the PD patterns in motors automatically [30–32].

The BCM is adopted for computing the fractal features of 3D images [33]. BCM is a method of gathering data for analysing complex patterns by breaking a dataset or image into smaller and smaller pieces, typically 'box'-shaped, and analysing the pieces at each smaller scale. The advantage of BCM is that it considers both the number of empty boxes and filled boxes. Besides, the size of the filled box is taken into consideration as well and the inhomogeneous character of the fractal image is well represented. In this paper, the BCM-based fractal analysis is applied to extract FD and lacunarity from 3D PPD pattern images.

4.2 Calculation of fractal features using the BCM

The basic procedure of BCM is to systematically lay a series of grids of decreasing the box sizes over an image and record data (the counting) for each successive size. In order to extract fractal features from 3D PPD pattern images, the steps are listed below:

- *Step 1:* To scale the box size, L. L is the side size of a 3D box in BCM to cover a fractal object [25]. With the decreasing of L, the measurements obtained become increasingly sensitive and lend to infinity if the L approaches 0. Here the determination of the value of L is based on the consideration of accuracy and the required computational effort, both of which increase with the maximum value of L. Theoretically, it is beneficial to examine as large a range of L ($L = 0, \ldots, L_{\max}$) as possible until $L_{\max}$ reaches the image dimension. In this work, $L_{\max}$ has been chosen as 128, the size of the pixel map of the PPD patterns.
- *Step 2:* To count the number of boxes $N(L)$. $P(m, L)$ is defined as the probability that there are m points within a box of size L. Accumulating the occurrences of neighbouring points over the image gives the frequency of occurrence, m. To calculate m, the boxes with different L are centred at each pixel of the image and m is the number of the points inside the box. The m is accumulated over the entire image to and normalised to obtain $P(m, L)$. For all L,$P(m, L)$ is normalised according to

$$\sum_{m=1}^{N} P(m, L) = 1 \tag{2}$$

where N is the number of possible points within the box.

$N(L)$ is defined as the expected total number of boxes needed to cover the whole image, as shown in

$$N(L) = \sum_{m=1}^{N} \frac{S}{m} P(m, L) \tag{3}$$

where S is the number of image points of PPD pattern.
- *Step 3:* To calculate FD. The actual size of the contents $N(L)$ is proportional to L^{-D} [26], as shown in

$$N(L) = \frac{1}{(L/L_{\max})^D} = \left(\frac{L}{L_{\max}}\right)^{-D} \propto L^{-D} \tag{4}$$

where $L_{\max}$ is the max value of L.

Consequently, the value of D can be estimated by least square fitting on $\{\log(L), -\log(N(L))\}$, for different values of L. The slope of the curve is the estimation of D.
- *Step 4:* To calculate lacunarity: Lacunarity is also a function of the box size L. The lacunarity Λ could be calculated based on the second-order statistics of $P(m, L)$ as shown in

$$M(L) = \sum_{m=1}^{N} m \cdot P(m, L) \tag{5}$$

$$M^2(L) = \sum_{m=1}^{N} m^2 \cdot P(m, L) \tag{6}$$

$$\Lambda(L) = \frac{M^2(L) - [M(L)]^2}{[M(L)]^2} \tag{7}$$

5 Fractal map of standard patterns

The proposed PRPD-to-PPD conversion and BCM-based fractal analysis have been applied to the six types of motor PD sources described in IEC 60034-27-2 [20], namely:

- internal void (denoted as PD 1 for future discussion);
- internal delamination (PD 2);
- delamination between conductor and insulation (PD 3);
- slot discharge (PD 4);
- surface discharge (PD 5);
- gap type discharge (PD 6).

Their 3D PRPD patterns, shown in the left-hand column of Fig. 2, form the pattern recognition standard in this work. Moreover, the 3D PRPD format is converted to 3D PPD patterns, as shown in the right-hand column of Fig. 2.

The individual 3D PPD pattern images, with a resolution of 128×128. x and y axes denote the polarised phase and normalised amplitude, respectively. z-axis denotes the pulse count data. The number of PD events at each x/y location is uniquely mapped to one of the 16 colours available.

In the proposed method in Section 4, 3D PPD pattern images are divided by box size, $L = 2^n$ ($n = 0, 1, \ldots, 7$). A total of eight groups of boxes are calculated. Then the fractal-based feature extraction is made to extract fractal dimension and lacunarity features from converted 3D PPD patterns.

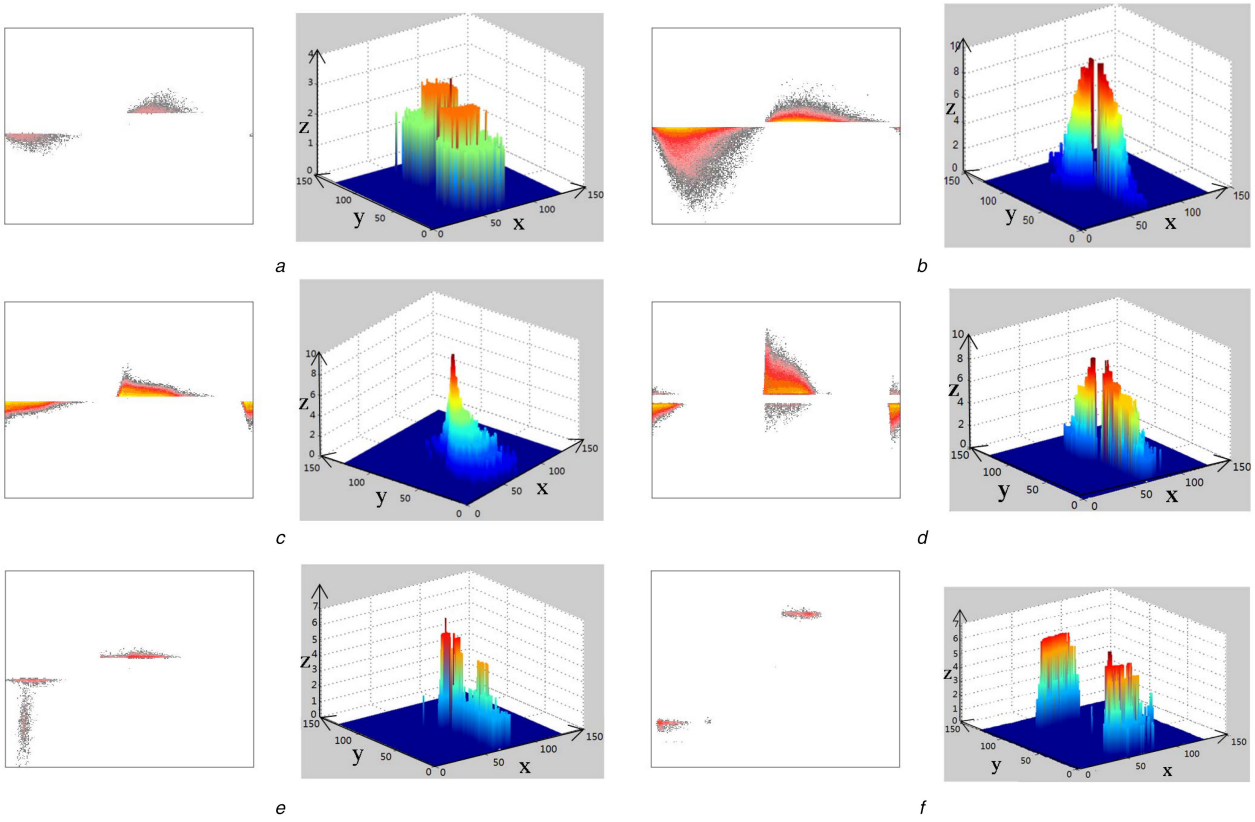

Fig. 2 *PRPD pattern image and PPD pattern image of six selected typical motor PD based on IEC standard*
(a) PD 1 (internal void discharge) PRPD pattern image and PPD pattern image, ***(b)*** PD 2 (internal delamination) PRPD pattern image and PPD pattern image, ***(c)*** PD 3 (delamination between conductor and insulation) PRPD pattern image and PPD pattern image, ***(d)*** PD 4 (slot discharge) PRPD pattern image and PPD pattern image, ***(e)*** PD 5 (surface discharge) PRPD pattern image and PPD pattern image, ***(f)*** PD 6 (gap type discharge) PRPD pattern image and PPD pattern image

Table 1 Fractal features of PPD images converted from standard

PD type	Fractal dimension (D)	Lacunarity (Λ)
1	2.5953	0.2484
2	2.4288	0.4491
3	2.3951	0.6523
4	2.4428	0.3996
5	2.3226	0.8008
6	2.3622	0.5552

5.1 Fractal map of single-source PD

Fractal features (D and Λ) of the converted 3D PPD images from the standard 3D PRPD patterns are calculated and shown in Table 1.

To consider the fact that PD activities and associated PD patterns rarely repeat themselves, even for the same defect site and for the same type of PD by a certain degree, 20 sets of data originated from each of the IEC standard PRPD pattern images by compressing and extending the pattern up to 30% were implemented in order to test the robustness of the proposed method.

Fig. 3 plots the clusters of fractal features of the converted PPD images after extension and compression. In Fig. 3, the darker points are the fractal parameters converted from unchanged standard PRPD image, as presented in Table 1; the lighter points are the clusters of fractal parameters after compression and extension.

In Fig. 4, the proposed method can separate the groups using fractal features. As shown, clusters belonging to a particular fault type are found to lie close to each other, and more significantly, most are reasonably well separated from other fault types. It is to be noticed that the fractal features of PD 2 and PD 4 overlap to a degree. That's because the PRPD images of these two PD types have a very similar shape: both polarities of PD 2 and PD 4 are a triangle, as presented in Fig. 4. The difference between PD 2 and PD 4 is in their symmetry. The triangles of PD 2 at each polarity are symmetric. This is because it is generated between insulation layers where the conductivity and permeability are same. The triangles of PD 4 at each polarity are asymmetric. This is because it is generated between the insulation layer and stator core where the conductivity and permeability are different. Since the risk associated with PD 2 and PD 4 is at a high level [34], it is highly recommended that a more detailed inspection of the motor is carried out once a PD fault with these fractal features is detected.

5.2 Fractal map of multiple-source PD

The double-source PDs are formed by various combinations of the six single-source PDs. The number of double-source PD sources formed is 15. The procedure of setting up the criteria for distinguishing double-source PD is similar to that described in the previous sections. Fig. 5 shows the 15 clusters of fractal features of the converted double-source PPD images after extension and compression.

In practical PD measurements, the multi-source PD problem is very common [15]. To investigate the ability of the proposed PD recognition techniques to recognise multi-source PDs, these 21 PD types form a fractal map shown in Fig. 5 to distinguish multi-source PD detected from the on-site test.

In Figs. 3 and 5, the clusters of fractal features of different PPD images are well separated but the boundary is very close to one

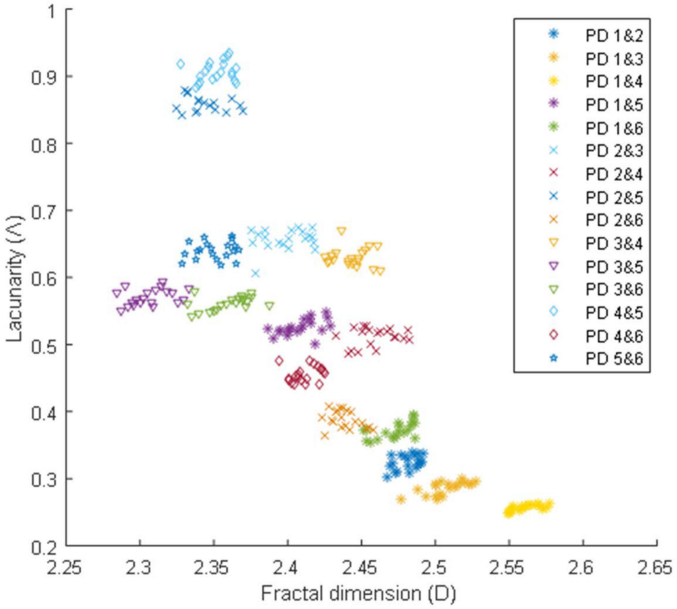

Fig. 3 *Cluster representation of the fractal map showing pattern discrimination capabilities for double-source PD*

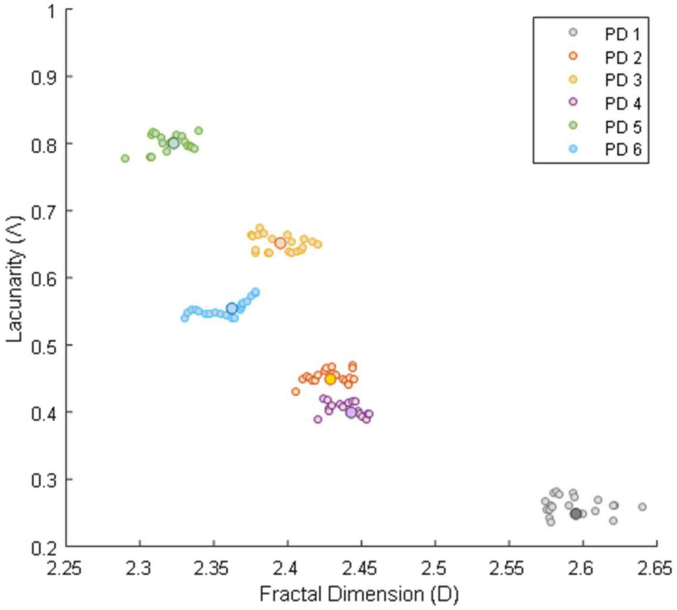

Fig. 4 *Cluster representation of the global D–Λ map showing pattern discrimination capabilities for single-source PD*

another, making it difficult to discriminate among double-source PDs. It is impossible to provide a reliable PD type classification method to specify the PD type(s) to one unidentified PD fault. In this paper, CS-based PD source classification is introduced to list the possibilities of each potential PD type to provide probability estimation.

6 CS algorithms for PD source classification

In order to determine whether a data set fits well with predefined fault information, the CS is developed. The CS is defined as the percentile rank of the distance between the fractal point of unknown defects and the centre of the defined fractal clusters. The fractal features of the defined PD patterns are displayed in a 2D space (D and Λ), as shown in Figs. 3–5. Taking Fig. 4 as an example, six clusters of defined single-source PD patterns are displayed in one map. The mathematical centre of each cluster is determined and the position of an unknown defect can be compared with this centre. The CS can vary from 0 to 100%. It reflects the probability of an unknown defect recognised as a defined PD pattern in the fractal map. The value of CS higher than 0 indicates a possible defined PD pattern in the fractal map; the value of CS equals to 0 indicates an unknown PD pattern.

The first step is to measure the distance between the fractal features of unknown defects and the average values of the fractal features of defined fractal clusters in the fractal map. The distance is calculated as

$$d_k^2 = \frac{(u-\mu)^2}{\sigma_k^2} \tag{8}$$

where u is the fractal feature (D and Λ) of the unknown defect; μ is the average value of all defined fractal clusters; σ_k is the standard deviation of a defined fractal cluster; k is the number of the PD types, $k = 1, \ldots, 21$.

The standard deviation of a defined fractal cluster is given as

$$\sigma_k^2 = \frac{1}{N}\sum_{i=1}^{N}(\mu_i - \mu)^2 \tag{9}$$

where N is the total number of fractal clusters, in this case, $N = 21$; μ_i is the average value of a defined fractal cluster.

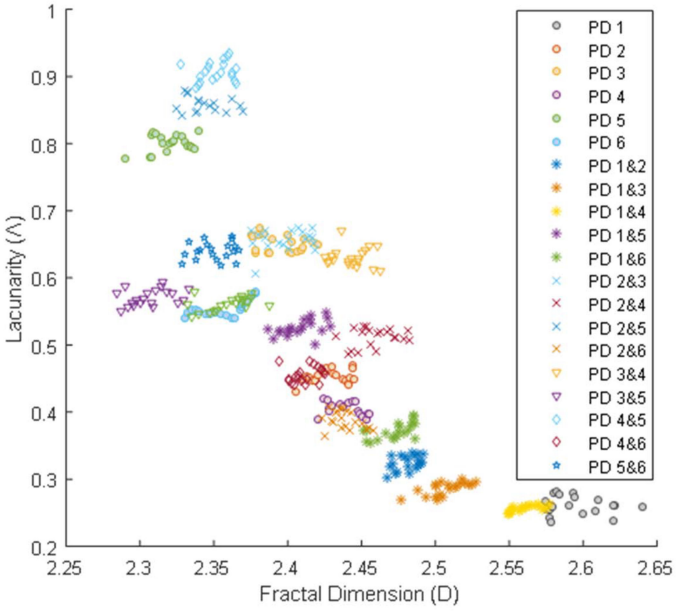

Fig. 5 *Cluster representation of the fractal map showing pattern discrimination capabilities for double-source and single-source PD*

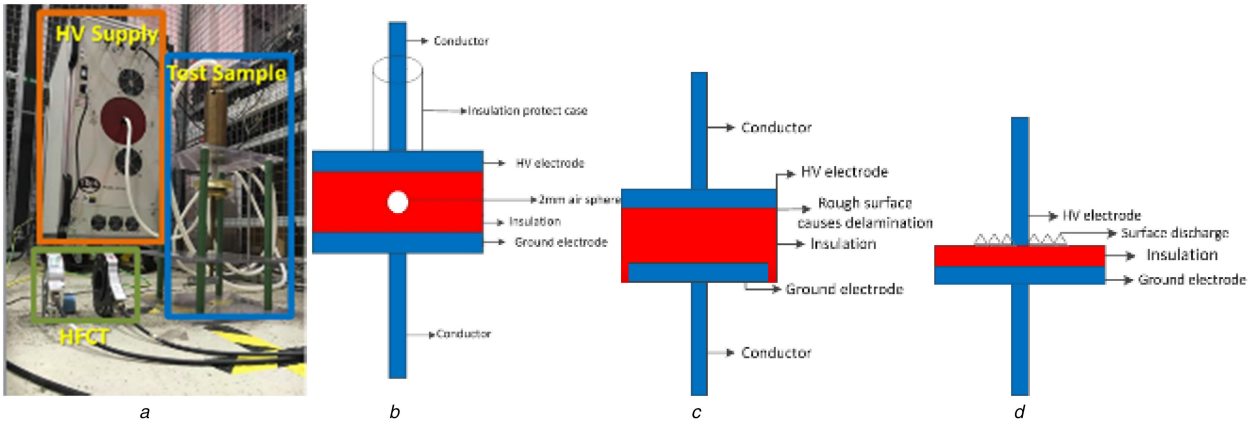

Fig. 6 *PD measurement experimental setup and PD geometries*

(a) Experiment setup, ***(b)*** PD 1 (internal void discharge)geometry setup for experiment, ***(c)*** PD 3 (delamination between conductor and insulation) geometry setup for experiment, ***(d)*** PD 5 (surface discharge) geometry setup for experiment

The covariance matrix can be considered to be a multi-dimensional generalisation of the 1D standard deviation. Finally, the CS is defined as

$$\mathrm{CS}_k = \left(100 - \mathrm{PR}_{d_k^2}\right)/100 \tag{10}$$

where PR is the percentile rank of $d_k{}^2$ as given as

$$\mathrm{PR} = \frac{c_l + 0.5 f_i}{N} \times 100\% \tag{11}$$

where c_l is the count of all scores less than the score of interest, f_i is the frequency of the score of interest, and N is the number of examinees in the samples.

The recognition rate is calculated based on the ratio between the recognised test sample and the sum of all test samples.

7 Experimental work for validation

7.1 Experimental setup

The experimental work completed aims to test the performance of the proposed algorithms including PD data pre-processing procedures, PRPD-to-PPD pattern conversion, fractal theory-based PPD pattern feature extraction, and CS-based classification. Because it is hard to generate and control the same PD types in a real motor, the experiment is carried on the simplified geometry to present the similar fault type inside a motor. The experiment setup for validation is depicted in Fig. 6. Function generator was used to generate 50 Hz sine wave, which was used as the input signal to a power amplifier to be amplified as power supply. A HFCT, with frequency response 50 kHz–20 MHz, is clamped around the ground wire to measure PD signal (as in on-site tests). Artificial faults are designed to simulate three types of PD sources, namely internal void discharge (denoted as PD 1), delamination between conductor and insulation discharge (denoted as PD 3), surface discharge (denoted as PD 5).

During the data acquisition, Channel 1 recorded the outputs from the HFCT while Channel 2 recorded the applied voltage as the phase reference. For each of the modelled faults, measurements were conducted for 20 times with each four times under one level of voltage supply. The lowest voltage supply is the PD inception voltage, and the higher-level voltage is 0.2 kV higher than lower level. At one acquisition, PD pulses are recorded over 500 power cycles. For each of three faults, 20 acquisitions are recorded and thus total 60 sets of discharge signal samples are used as test data for evaluating the algorithms presented in this paper.

7.2 Result and analysis

7.2.1 Single-source PD pattern recognition: Fig. 7 shows the single-source PD recognition results when applying the introduced experiment setup and data pre-processing procedures to the experimental data.

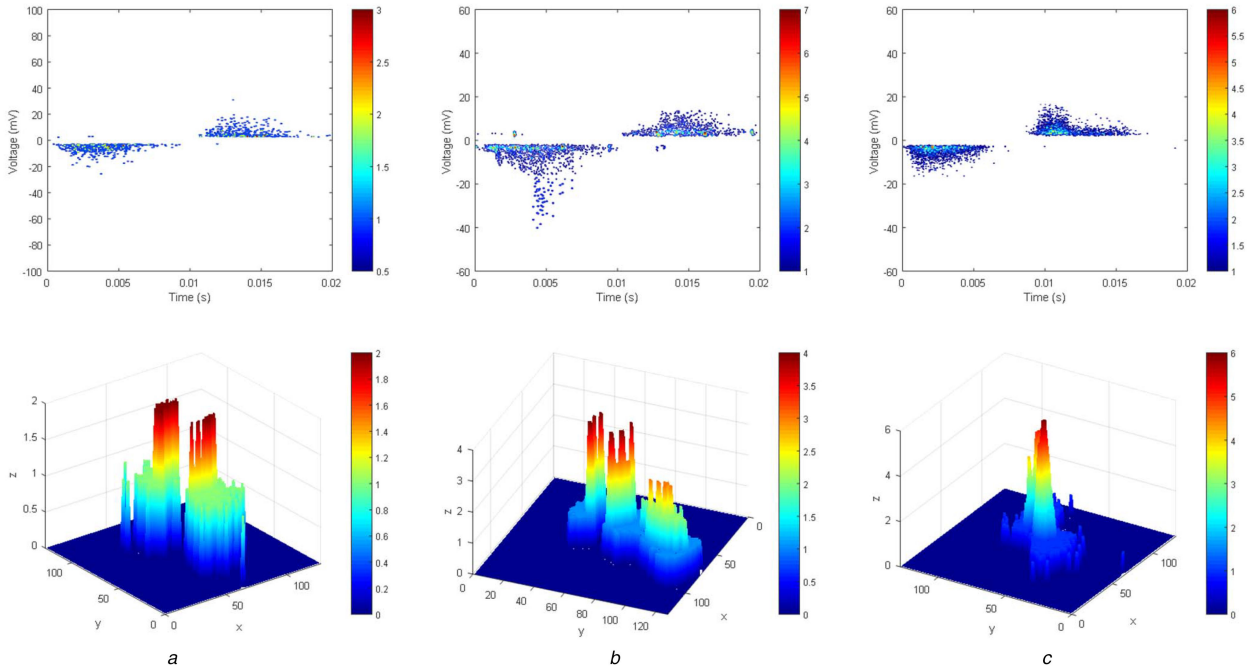

Fig. 7 *PRPD patterns and PPD patterns of three PD geometries*

(a) PRPD pattern and PPD pattern of the experimental result of PD1, ***(b)*** PRPD pattern and PPD pattern of the experimental result of PD3, ***(c)*** PRPD pattern and PPD pattern of the experimental result of PD 5

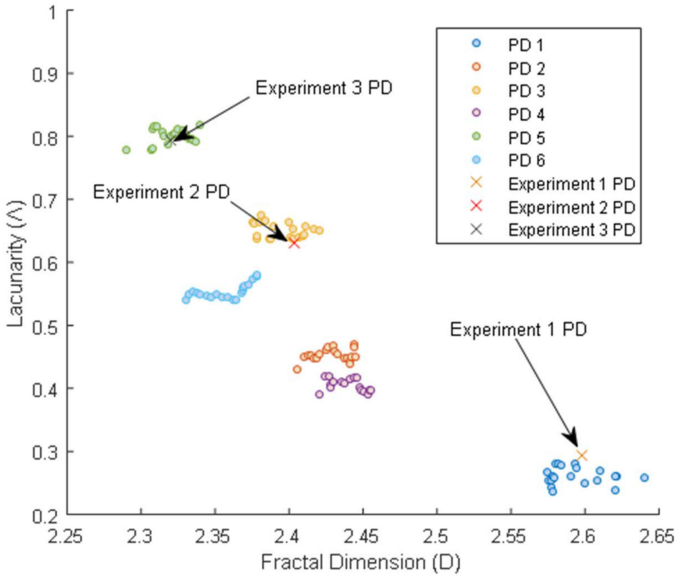

Fig. 8 *Cluster representation on the global D–Λ map showing single PD source experimental results*

The fractal map as shown in Fig. 4 in Section 5.1 is applied to the CS-based pattern classification algorithm for the probability estimation of PD source type. The fractal features are extracted from the 3D PPD patterns shown in Fig. 7 and are displayed in the fractal map in Fig. 8.

The fractal analysis results for the single-source PDs are shown in Fig. 8. It is clearly that the PD type in experiment 1 was correctly recognised as PD 1 (internal void discharge); the PD type in experiment 2 was correctly recognised as PD 3 (delamination between conductor and insulation); the PD type in experiment 3 was correctly recognised as PD 5 (surface discharge).

The recognition results based on the CS method are in Table 2. It shows 3 sets of experiments, each with 20 sets of data. In experiment 1, due to the fractal clusters PD 1 and PDs 1 & 4 are close in fractal map shown in Fig. 5, the CS results of PDs 1 and 4 are also demonstrated in Table 2. In considering the fact that 19 sets of CS results of PD 1 are above 0, the recognition rate of PD 1 in experiment 1 is 95%. This is applicable in other PD type recognition. The recognition rates of single-source PD in these three experiments are not <90%. However, due to the overlap between clusters in multi-source fractal map in Fig. 5, the CS results are able to provide the probabilities for all possible defined PD types. The higher CS is, the more likely this PD pattern is.

7.2.2 Double-source PD pattern recognition: To validate the application of the proposed method to double-source PD recognition, three artificial data sets are generated by combining the PD data from two of the experimental arrangements, as follows:

i. Superposing the PRPD patterns of experiments 1 and 2 (PDs 1 and 3).
ii. Superposing the PRPD patterns of experiments 1 and 3 (PDs 1 and 5).
iii. Superposing the PRPD patterns of experiments 2 and 3 (PDs 3 and 5).

Table 2 Classification results of the proposed method in single PD recognition when applied to experimental result

Test group	Experiment 1 (PD 1)				Experiment 2 (PD 3)				Experiment 3 (PD 5)			
	Fractal features		Potential PD (CS)		Fractal features		Potential PD (CS)		Fractal features		Potential PD (CS)	
	D	Λ	PD 1, %	PDs 1 and 4, %	D	Λ	PD 3, %	PDs 2 and 3, %	D	Λ	PD 5, %	PDs 2 and 5, %
1	2.5576	0.2586	0	15	2.3560	0.6428	0	0	2.3029	0.7946	5	0
2	2.5634	0.2592	5	15	2.3651	0.6430	15	0	2.3105	0.8119	10	0
3	2.5724	0.2846	10	45	2.3655	0.6438	15	0	2.3152	0.8073	55	0
4	2.5756	0.2452	10	20	2.3662	0.6428	15	5	2.3153	0.8068	75	0
5	2.5789	0.2675	20	15	2.3680	0.6421	10	5	2.3168	0.8081	65	0
6	2.5806	0.2614	25	10	2.3680	0.6403	10	0	2.3172	0.8070	60	0
7	2.5851	0.2681	30	5	2.3703	0.6411	10	0	2.3199	0.8124	80	0
8	2.5907	0.2458	40	10	2.3773	0.6461	30	20	2.3202	0.7931	90	0
9	2.5916	0.2843	65	15	2.3788	0.6453	45	30	2.3227	0.8024	75	0
10	2.5920	0.2840	65	15	2.3854	0.6249	85	80	2.3227	0.8083	85	0
11	2.6010	0.2953	80	5	2.3859	0.6237	90	75	2.3257	0.7963	70	0
12	2.5983	0.2927	80	5	2.3983	0.6477	65	80	2.3268	0.8117	45	0
13	2.6005	0.2514	75	5	2.4027	0.6283	80	40	2.3308	0.8207	65	0
14	2.6009	0.2509	75	5	2.4033	0.6308	80	40	2.3416	0.8003	40	0
15	2.6124	0.2627	20	0	2.4136	0.6381	65	15	2.3421	0.7883	10	5
16	2.6135	0.2622	20	0	2.4094	0.6289	60	15	2.3430	0.7905	25	0
17	2.6133	0.2718	10	0	2.4086	0.6308	35	0	2.3442	0.7972	20	0
18	2.6145	0.2720	10	0	2.4113	0.6319	20	5	2.3450	0.8215	20	15
19	2.6271	0.2722	5	0	2.4208	0.6193	5	0	2.3453	0.8207	10	15
20	2.6280	0.2914	5	0	2.4320	0.6342	0	0	2.3507	0.7821	0	0
average			32.5	8.75			36.75	20.5			45.25	1.75
							recognition rate					
	PD 1 (95%) might also be PDs 1–4 (75%)				PD 3 (90%) might also be PDs 2 and 3 (60%)				PD 5 (95%) might also be PDs 2–5 (15%)			

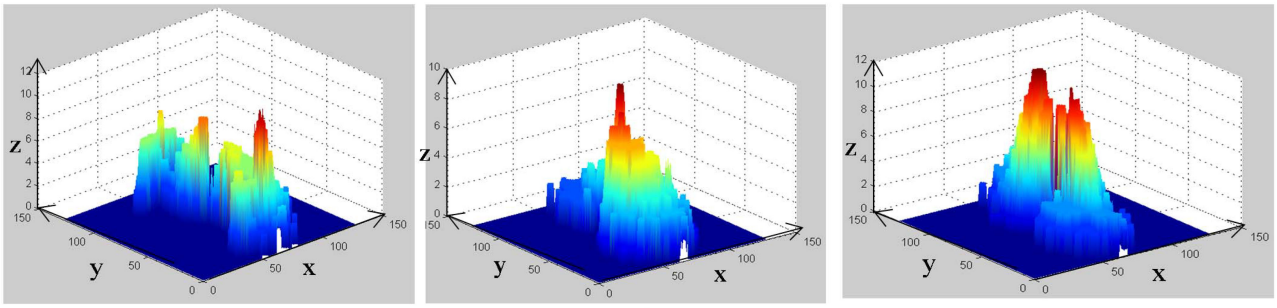

Fig. 9 *PPD pattern image of double-source PD samples*

(a) PDs 1 and 3 PPD pattern based on the results of experiments 1 and 2, ***(b)*** PDs 1 and 5 PPD pattern based on the results of experiments 1 and 3, ***(c)*** PDs 3 and 5 PPD pattern based on the results of experiments 2 and 3

Due to the reference voltage signal was applicable in lab condition, it was possible to combine different PRPD patterns to generate a double-source PD pattern to test the feasibility of the proposed methods. Fig. 9 shows the 3D PPD patterns of the three double-source PDs.

The fractal analysis results for the double-source PDs are shown in Fig. 10. It is clearly that the PD type from the combined PRPD patterns of experiments 1 and 2 was correctly recognised as the PDs 1 and 3 (blue circle in Fig. 10); the PD type from the combined PRPD patterns of experiments 1 and 3 was correctly recognised as the PDs 1 and 5 (red circle in Fig. 10); the PD type from the combined PRPD patterns of experiments 2 and 3 was correctly recognised as the PDs 3 and 5 (yellow circle in Fig. 10).

The recognition results based on the CS method are in Table 3. It shows 3 sets of results from the combined PRPD pattern, each with 20 sets of data. In the results of combined experiments 1 and 2, due to the fractal clusters PDs 1 and 3 and PDs 1 and 2 are close in fractal map shown in Fig. 5, the CS results of the PDs 1 and 2 are also demonstrated in Table 3. In considering the fact that 16 sets of CS results of PD 1 are above 0, the recognition rate of PDs 1 and 3 is 95% in this combined experimental result. This is applicable in other PD type recognition. The recognition rates of single-source PD in these three experiments are not <80%.

8 Applications to practical on-site test data

The proposed method is applied to the practical situation of on-site test of three-phase industrial motors. The test data was collected at a number of nuclear power stations, using HFCTs clamped around the earth strips of the motor supply cables. The installation of the current sensor in field is illustrated in Fig. 11, where, the applied current sensors are installed at the earth strip below the switchboard. The benefit of the use of HFCT is that it, due to its good frequency bandwidth, is capable of detecting PD emanating from local switchgear, from cable and from cooling water pump motor which is usually 300–500 m away. PD was detected from four MV motors (A, B, C and D) and recorded for later analysis.

Fig. 12 shows the PRPD pattern of tested motors. By visual inspection of the PRPD patterns in comparison with standard PD patterns as given in IEC60034-27, the fault in motor A might be PD 1 (internal void discharge); the PD pattern of motor B might be double-source PD 4 and 5 (slot discharge and surface discharge);

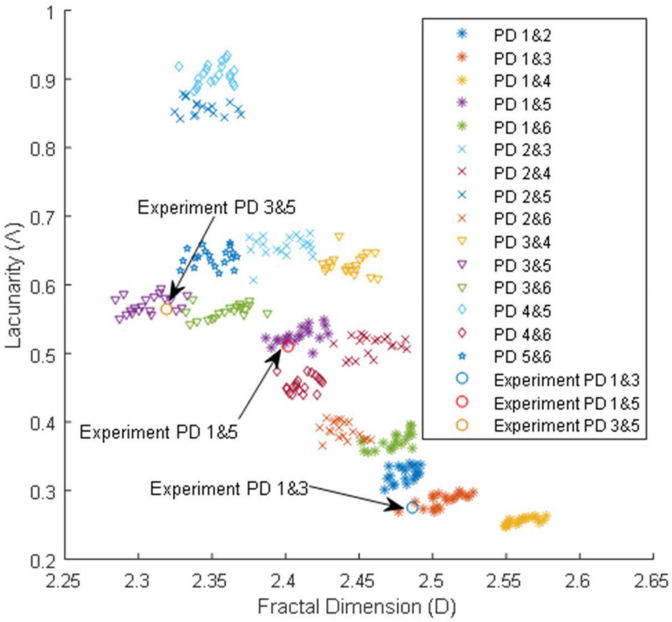

Fig. 10 *Cluster representation on the global D–Λ map showing double-source PD experimental results*

Table 3 Classification results of the proposed method in double-source PD recognition when applied to experimental result

Test group	Combined experiment result in PDs 1 and 3				Combined experiment result in PDs 1 and 5				Combined experiment result in PDs 3 and 5				
	Fractal features		Potential PD (CS)		Fractal features		Potential PD (CS)		Fractal features		Potential PD (CS)		
	D	Λ	PDs 1 and 3, %	PDs 1 and 2, %	*D*	Λ	PDs 1 and 5, %	PDs 4 and 6, %	*D*	Λ	PDs 3 and 5, %	PDs 3 and 6, %	PD 6, %
1	2.4667	0.3054	0	10	2.3754	0.5281	0	0	2.2780	0.5537	0	0	0
2	2.4688	0.3130	5	25	2.3781	0.5233	20	0	2.2831	0.5861	0	0	0
3	2.4865	0.2752	15	5	2.3796	0.4882	25	20	2.2957	0.5456	10	0	0
4	2.4883	0.3217	20	20	2.3821	0.5067	10	0	2.3049	0.5513	15	0	0
5	2.4907	0.2865	25	0	2.3901	0.5116	25	0	2.3057	0.5716	20	0	0
6	2.4921	0.3108	20	0	2.3926	0.5097	35	0	2.3092	0.5483	15	0	0
7	2.5013	0.3032	85	0	2.4017	0.5113	65	0	2.3144	0.5817	30	0	0
8	2.5039	0.2957	85	0	2.4021	0.5081	65	0	2.3147	0.5394	25	0	0
9	2.5077	0.3198	75	0	2.4097	0.5207	80	0	2.3193	0.5645	90	0	0
10	2.5100	0.2883	70	0	2.4100	0.5031	70	0	2.3202	0.5837	45	0	0
11	2.5108	0.3084	75	0	2.4106	0.4833	25	15	2.3217	0.5693	50	0	0
12	2.5166	0.3167	70	0	2.4119	0.4901	25	15	2.3223	0.5509	55	0	0
13	2.5168	0.2937	60	0	2.4203	0.5117	35	0	2.3225	0.5229	20	0	0
14	2.5197	0.3056	35	0	2.4231	0.5129	10	0	2.3247	0.5694	45	0	0
15	2.5208	0.3288	15	0	2.4236	0.5089	10	0	2.3279	0.5701	15	0	0
16	2.5213	0.3279	15	0	2.4259	0.5109	5	0	2.3281	0.5327	15	0	0
17	2.5245	0.2991	10	0	2.4280	0.5277	5	0	2.3327	0.5617	5	0	0
18	2.5273	0.3057	0	0	2.4288	0.4937	10	0	2.3329	0.5509	5	0	0
19	2.5288	0.2871	0	0	2.4296	0.5110	0	0	2.3371	0.5392	0	5	0
20	2.5292	0.3104	0	0	2.4327	0.5226	0	0	2.3392	0.5726	0	10	5
average			34	3			26	2.5			23	0.75	0.25
	recognition rate												
	PDs 1–3 (80%) might also be PDs 1 and 2 (20%)				PDs 1–5 (85%) might also be PDs 4–6 (15%)				PDs 3–5 (80%) might also be PDs 3–6 (10%), PD 6 (5%)				

the PD pattern of motor *C* might be PD 1 (internal void discharge); and the PD pattern of motor *D* might be PD 4 (slot discharge). It is to be noted that the authors do not have photographs to show the evidential damage of the defect site (Fig. 13).

The proposed pattern recognition algorithm was applied to these four motors. The recognition results were shown in Table 4. The recognition results agree well with the visual inspection. The recognition rate for multi-source PD is not <86.7% in practical situations. The CS-based pattern classification shows all potential PD patterns with a ranked score. Take Motor D, for example the PD pattern recognition result is PD 4 with the recognition rate 100%, PDs 2 and 6 with recognition rate 83%, PD 2 with recognition rate 83%, which all have high possibilities. When considering the average CS, the average value of CS of PD 4 is much higher than the other two patterns. It indicates the tested PD pattern is more likely to be PD 4.

9 Conclusion

This paper described a combination of theoretical and practical study into the feasibility of using fractal theory to discriminate multiple motor PD sources. PRPD patterns were modified to create

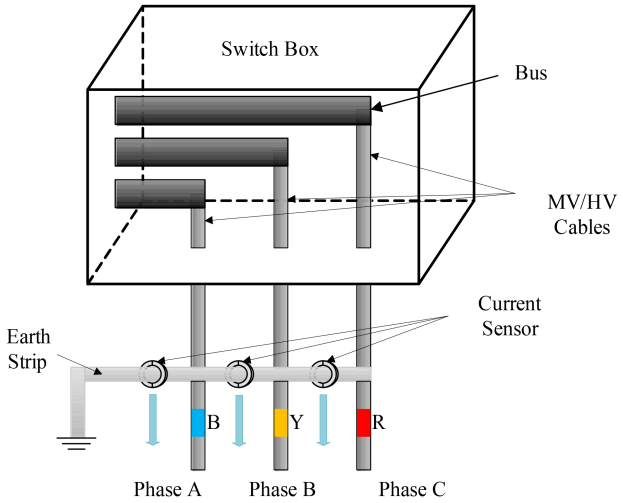

Fig. 11 *Installation of HFCTs in field test*

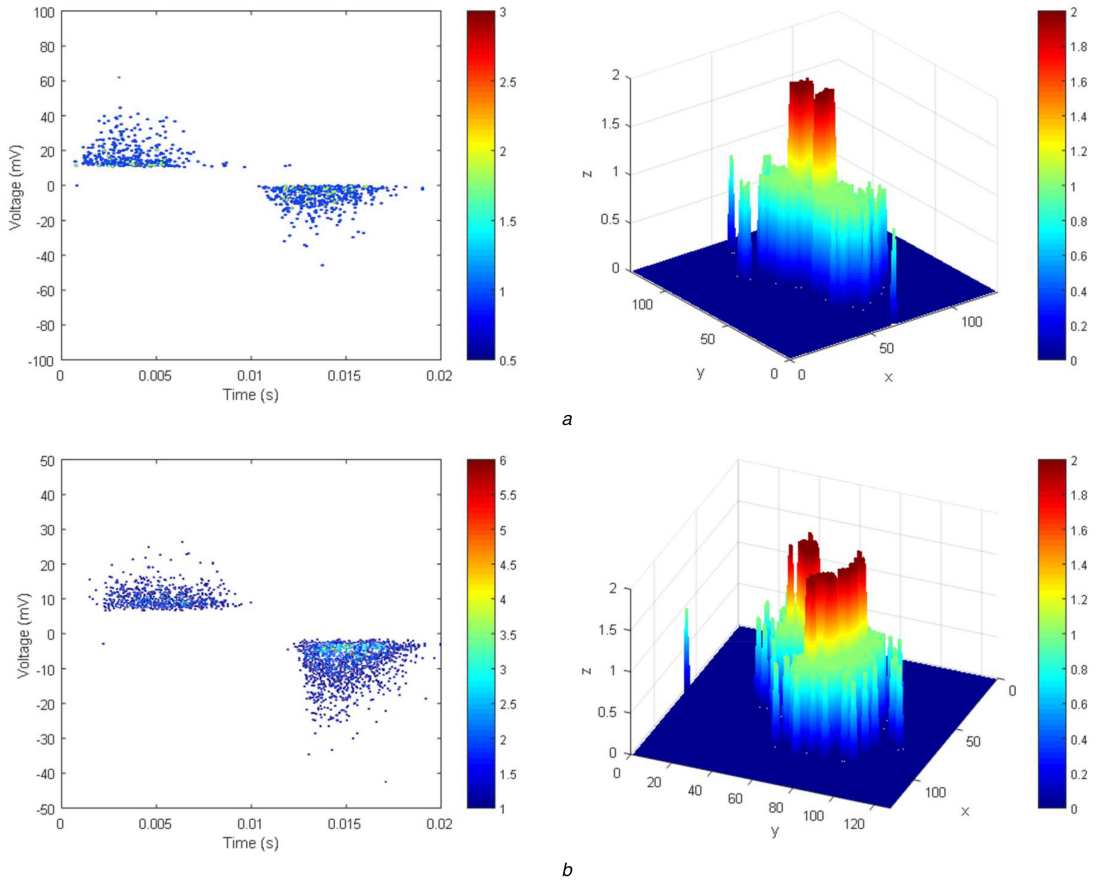

Fig. 12 *Continued*

polar PD patterns to address the problem of lack of voltage phase information. Two fractal features, fractal dimension D and lacunarity Λ, were employed to measure the shapes of PPD. The reference PPD patterns were created from the PRPD patterns in IEC 60034-27-2. The fractal maps of single-source PDs and double-source PDs showed good stability when the shapes of PPD patterns were compressed and extended. Three types of PD geometries were built and tested under laboratory conditions to validate the proposed method's pattern recognition performance for both single-source PDs and double-source PDs. Four sets of motor PD from on-site data were visually assessed and analysed in the fractal map of single-source PDs and double-source PDs. The recognition results agree well with the visual inspection.

The limitation is that several clusters of PPD patterns are very close in the fractal map, which may cause incorrect identification. However, the ones close to each other have similar risk level in terms of further degradation. A risk-based diagnosis will be investigated as future work.

10 Acknowledgments

The authors thank EDF Energy for funding this project.

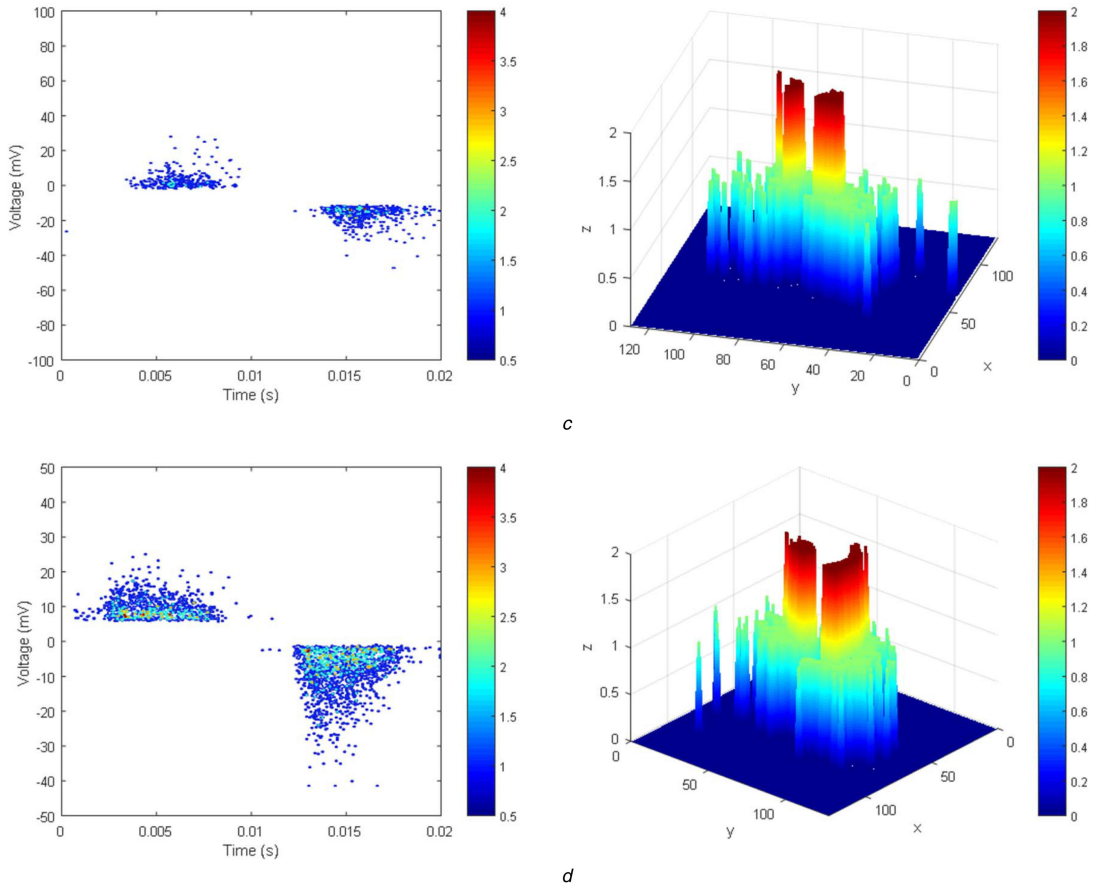

Fig. 12 *PRPD pattern and the PPD pattern images of motors A, B, C and D*

(a) PRPD pattern and the PPD pattern image of motor *A*, ***(b)*** PRPD pattern and the PPD pattern image of motor *B*, ***(c)*** PRPD pattern and the PPD pattern image of motor *C*, ***(d)*** PRPD pattern and the PPD pattern image of motor *D*

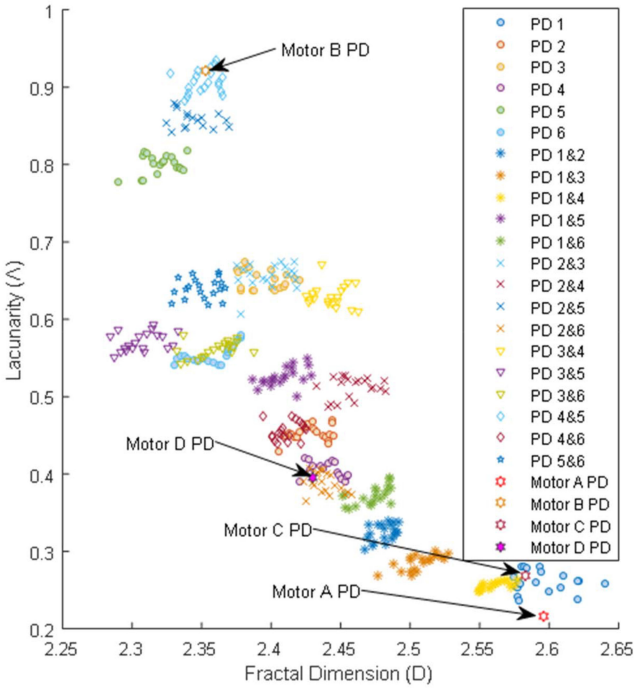

Fig. 13 *Cluster representation on the global D–Λ map showing double-source PD experimental results*

Table 4 Classification results of the proposed method in multi-source PD recognition when applied to on-site tests

Test group	Motor *A*				Motor *B*			
	Fractal features		Potential PD (CS)		Fractal features		Potential PD (CS)	
	D	Λ	PD 1, %	PDs 1 and 4, %	*D*	Λ	PD 4 and 5, %	PD 2 and 5, %
1	2.5726	0.2156	30	25	2.3357	0.9042	5	20
2	2.5742	0.2623	25	15	2.3436	0.9127	25	5
3	2.5832	0.2128	40	0	2.3479	0.9824	0	0
4	2.5957	0.2473	85	0	2.3527	0.9211	40	0
5	2.6283	0.2506	70	0	2.3583	0.9046	35	0
6	2.6363	0.2633	10	0	2.3771	0.8997	15	5
average			43.3	6.7			20	5
				recognition rate				
	PD 1 (100%), might also have PD 4 (33%)				PDs 4 and 5 (86.6%), might also have PD 2 (33%)			

Test group	Motor *C*				Motor *D*				
	Fractal features		PD code (CS)		Fractal features		PD (CS)		
	D	Λ	PD 1, %	PDs 1 and 4, %	*D*	Λ	PD 4, %	PDs 2 and 6, %	PD 2, %
1	2.5831	0.2693	80	10	2.4275	0.4246	40	10	5
2	2.5997	0.2532	75	0	2.4291	0.3882	20	40	0
3	2.6001	0.2551	75	0	2.4295	0.3956	75	80	0
4	2.6083	0.2752	30	0	2.4347	0.3819	60	10	0
5	2.6127	0.2382	30	0	2.4426	0.4176	20	0	15
6	2.6142	0.2401	30	0	2.4485	0.4058	30	25	0
average			53.3	1.7			41	27.5	3.3
					recognition rate				
	PD 1 (100%) might also have PD 4 (16.7%)				PD 4 (100%) might also have PDs 2 and 6 (83%), PD 2 (33.3%)				

11 References

[1] Stone, G.: 'The use of partial discharge measurements to assess the condition of rotating machine insulation', *IEEE Electr. Insul. Mag.*, 1996, **12**, (4), pp. 23–27

[2] Kheirmand, A., Leijon, M., Gubanski, S.M.: 'Advances in online monitoring and localization of partial discharges in large rotating machines', *IEEE Trans. Energy Convers.*, 2004, **19**, pp. 53–59

[3] Krivda, A.: '*Recognition of discharges: discrimination and classification*' (Delft University Press, Delft, 1995), pp. 41–53

[4] Zhou, C., Yi, H., Dong, X.: 'Review of recent research towards power cable life cycle management', *High Volt.*, 2017, **2**, (3), pp. 179–187

[5] Li, S., Nie, Y., Li, J.: 'Condition monitoring and diagnosis of power equipment: review and prospective', *High Volt.*, 2017, **2**, (2), pp. 82–91

[6] Sahoo, N.C., Salama, M.M.A., Bartnikas, R.: 'Trends in partial discharge pattern classification: a survey', *IEEE Trans. Dielectr. Electr. Insul.*, 2005, **12**, pp. 248–264

[7] Xiaoxing, Z., Jiangbo, R., Ju, T., *et al.*: 'Kernel statistical uncorrelated optimum discriminant vectors algorithm for GIS PD recognition', *IEEE Trans. Dielectr. Electr. Insul.*, 2009, **16**, pp. 206–213

[8] Cacciari, M., Contin, A., Montanari, G.C.: 'Use of a mixed-Weibull distribution for the identification of PD phenomena [rotating machines]', *IEEE Trans. Dielectr. Electr. Insul.*, 1995, **2**, pp. 614–627

[9] Gulski, E.: 'Digital analysis of partial discharges', *IEEE Trans. Dielectr. Electr. Insul.*, 1995, **2**, pp. 822–837

[10] Gulski, E.: 'Discharge pattern recognition in high voltage equipment'. 1993 Int. Conf. Partial Discharge, Canterbury, 1993, pp. 36–38

[11] Xiaoxing, Z., Song, X., Na, S., *et al.*: 'GIS partial discharge pattern recognition based on the chaos theory', *IEEE Trans. Dielectr. Electr. Insul.*, 2014, **21**, pp. 783–790

[12] Cavallini, A., Montanari, G., Fabiani, D., *et al.*: 'Advanced technique for partial discharge detection and analysis in power cables'. Int. Conf. Condition Monitoring & Diagnostic Engineering Management of Power Station/ Substation Equipment, 2009, pp. 1–4

[13] Lalitha, E.M., Satish, L.: 'Wavelet analysis for classification of multi-source PD patterns', *IEEE Trans. Dielectr. Electr. Insul.*, 2000, **7**, pp. 40–47

[14] Ma, H., Chan, J.C., Saha, T.K., *et al.*: 'Pattern recognition techniques and their applications for automatic classification of artificial partial discharge sources', *IEEE Trans. Dielectr. Electr. Insul.*, 2013, **20**, pp. 468–478

[15] Danikas, M., Gao, N., Aro, M.: 'Partial discharge recognition using neural networks: a review', *Electr. Eng.*, 2003, **85**, (2), pp. 87–93

[16] Oskuoee, M., Yazdizadeh, A.R., Mahdiani, H.R.: 'A new feature extraction and pattern recognition of partial discharge in solid material by neural network'. 2012 Eighth Int. Conf. Natural Computation (ICNC), 2012, pp. 183–187

[17] Kranz, H.-G.: 'Diagnosis of partial discharge signals using neural networks and minimum distance classification', *IEEE Trans. Electr. Insul.*, 1993, **28**, pp. 1016–1024

[18] Salama, M., Bartnikas, R.: 'Fuzzy logic applied to PD pattern classification', *IEEE Trans. Dielectr. Electr. Insul.*, 2000, **7**, pp. 118–123

[19] Xiaosheng, P., Chengke, Z., Hepburn, D.M., *et al.*: 'Application of K-means method to pattern recognition in on-line cable partial discharge monitoring', *IEEE Trans. Dielectr. Electr. Insul.*, 2013, **20**, pp. 754–761

[20] IEC TS 60034-27-2:2012: 'Rotating electrical machines – part 27-2: on-line partial discharge measurements on the stator winding insulation of rotating electrical machines', 2012

[21] Zhou, C., Hepburn, D.M., Song, X., *et al.*: 'Application of denoising techniques to PD measurement utilising UHF, HFCT, acoustic sensors and IEC60270'. CIRED 2009 – 20th Int. Conf. and Exhibition on Electricity Distribution – Part 1, Prague, Czech Republic, 2009, pp. 1–4

[22] Song, X., Zhou, C., Hepburn, D.M., *et al.*: 'Second generation wavelet transform for data denoising in PD measurement', *IEEE Trans. Dielectr. Electr. Insul.*, 2007, **14**, (6), pp. 1531–1537

[23] Mandelbrot, B.: '*The fractal geometry of nature*' (W.H. Freeman and Company, New York, 1982), pp. 166–180

[24] Chen, S.S., Keller, J.M., Crownover, R.M.: 'On the calculation of fractal features from images', *IEEE Trans. Pattern Anal. Mach. Intell.*, 1993, **15**, (10), pp. 1087–1090

[25] Keller, J.M., Chen, S., Crownover, R.M.: 'Texture description and segmentation through fractal geometry', *Comput. Vis. Graph. Image Process.*, 1989, **45**, pp. 150–166

[26] Satish, L., Zaengl, W.S.: 'Can fractal features be used for recognizing 3-d partial discharge patterns', *IEEE Trans. Dielectr. Electr. Insul.*, 1995, **2**, pp. 352–359

[27] Candela, R., Mirelli, G., Schifani, R.: 'PD recognition by means of statistical and fractal parameters and a neural network', *IEEE Trans. Dielectr. Electr. Insul.*, 2000, **7**, pp. 87–94

[28] Jian, L., Caixin, S., Grzybowski, S., *et al.*: 'Partial discharge image recognition using a new group of features', *IEEE Trans. Dielectr. Electr. Insul.*, 2006, **13**, pp. 1245–1253

[29] Krivda, A., Gulski, E., Satish, L., *et al.*: 'The use of fractal features for recognition of 3-D discharge patterns', *IEEE Trans. Dielectr. Electr. Insul.*, 1995, **2**, pp. 889–892

[30] Keller, J.M., Balghonaim, A.S.: 'A maximum likelihood estimate for two-variable fractal surface', *IEEE Trans. Image Process.*, 1998, **7**, (12), pp. 1746–1753

[31] Li, J., Sun, C., Li, X., *et al.*: 'Partial discharge pattern recognition using fractal dimension'. Proc. of 2001 Int. Symp. Electrical Insulating Materials, 2001 (ISEIM 2001), 2001, pp. 137–140

[32] Kreuger, F.F.H., Gulski, E., Krivda, A.: 'Classification of partial discharges', *IEEE Trans. Electr. Insul.*, 1993, **28**, (6), pp. 917–931

[33] Sarkar, N., Chaudhuri, B.B.: 'An efficient differential box-counting approach to compute fractal dimension of image', *IEEE Trans. Syst. Man Cybern.*, 1994, **24**, pp. 115–120

[34] IEEE Std 1434-2014: 'IEEE guide for the measurement of partial discharges in AC electric machinery', 2014